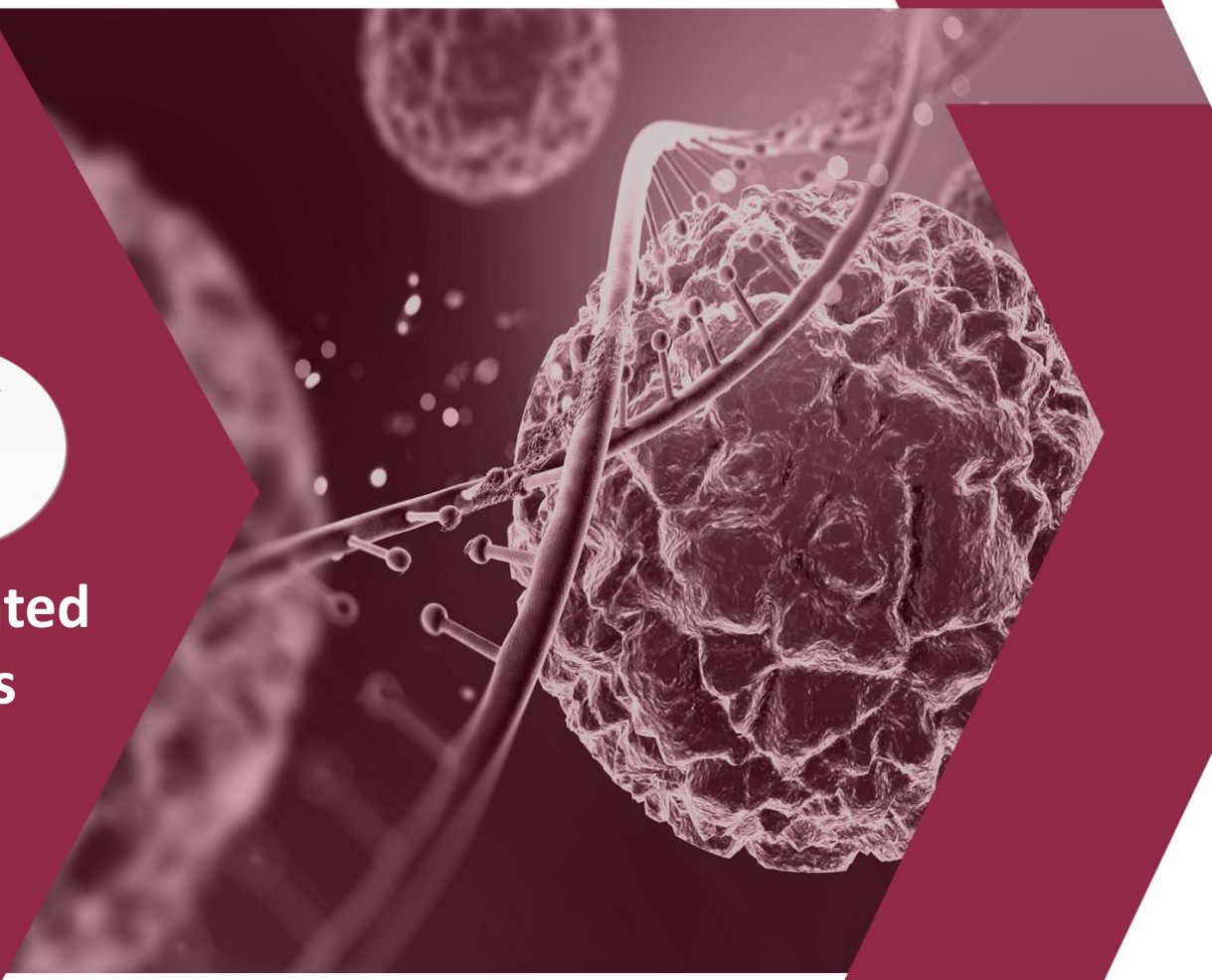

Underrated Nerds

Using PDEs to describe tumor growth

Technical Center for Career Development ICCD

Cairo University

Faculty of Engineering

Instructor:
Dr. Samah El-Tantawy

Table Of Contents

Content	Page #
Abstract	3
Introduction	3
Literature review	4-7
Mathematical Modeling	7
ODE modelling	7-8
PDE modelling	9-13
Solution and Analysis	14
The Gatenby-Gawlinski model	14-15
Numerical Solution and algorithm:	15-20
Multidimensional simulation	20
One-dimensional simulation	20-24
Two-dimensional simulation	26-28
Three-dimensional simulation	28-31
references	31

Table Of Figures

Figure #	Description	Page #
1	Analysis with change of the parameter d	**22**
2	Analysis with change of the parameter r	**22**
3	The numerical simulations	**23**
4	Front evolution & wave speed	**24**
5	Comparison between homogenous and heterogenous analysis	**25**
6	2D cells initial profile	**26**
7	2D homogenous invasion	**27**
8	2D heterogenous invasion	**27**
9	2D gap formation	**28**
10	3D density at initial & intermediate time	**28**
11	3D density	**29**
12	3D density half-ball	**30**
13	Figure11(B) and Figure 12(A),	**31**

Abstract

Mathematical modeling of biological systems especially on cancer has received much attention in recent times because it can reduce the complicated and costly experimental procedures. In addition to the fact that simulation of cancer behavior across multiple biological scales in space and time is a powerful tool that enables more accurate predictions, the cells evolve through different premalignant stages to become invasive and degrade the extracellular matrix (ECM) or surrounding tissue. In those papers we will discuss how mathematical modeling in this topic has evolved through the years.

Introduction

As our world's population is ever increasing, naturally there would be a rise in cancer cases, as 39.5% of men and women will be diagnosed with cancer at some point during their lifetimes (based on 2015–2017 data) [i]. Therefore, an accurate mathematical model of the growth of cancer tumors is a necessity now more than ever, so that we could compare it with different treatment methods and measure their effectivity.

Although using mathematical models to simulate biological processes is nothing new, creating a mathematical model for tumor growth could be tricky due to the several factors affecting the growth of tumors, e.g., the natural death of cancer cells, the host carrying capacity and the dichotomous actions of the immune response, are all factors that induce significant variations in tumor growth dynamics that mathematical modeling can help to understand.

The use of ordinary differential equations was a common practice in most literatures, and ordinary differential equation models have proven to be a useful

tool to simulate the evolution of total tumor cell number over time, but the most apparent shortcoming of this approach is the lack of spatial consideration. Patients never die because of the total number of cancer cells in their body, but because the primary tumors locally invade the tissue and spread (metastasize) to distant sites of the body to establish secondary tumors.

Hence the usage of partial differential equations allows us to represent cancer invasion and the metastatic spread, which are two crucial and inherently spatial processes in the growth and spread of tumors.

Literature view

We will start with 1998 [2]

(Growth of non-necrotic tumors in the presence and absence of inhibitors)

They have considered Byrne and Chaplain's model for the radial growth of non-necrotic, vascular tumors in the absence of Inhibitors.

In doing so, they developed the mathematical techniques for a rigorous analysis of transient and stationary solutions to such free boundary models. In the particular case under consideration, these techniques allowed us to confirm, extend, and sometimes rectify, the results that were obtained in [3] through asymptotic and numerical studies. They were able to achieve some results as:

1-Once the tumor is endangered, it will grow (according to the mathematical model) by 283 times.

2- they showed that the model predicts the exponential convergence of the nutrient concentration and tumor size to the nontrivial stationary solution, regardless of the initial conditions.

In 2012, Zentrum Mathematik, Technische Universität München BoltzmannStr. 3, 85748 Garching b. München, Germany.

(Delay equations modeling and immunotherapy on proliferating tumor cells)

In this paper they put the main cause of cancer is a malfunction of the control system, which leads to uncontrolled growth of a group of cells.

They give a mathematical model for tumor growth based on the dynamics of the cell cycle and derive their model from a renewal equation (set of differential equations with delay).

As a further improvement on the existing delay models, they also ensure positive of solutions, choosing the initial functions from a proper set of initial data.

A similar modeling approach has also been used in [4][5] .In both works, mathematical models were developed using the mass action principle, which combined with the delay equation approach leads to incorrectness in the equations.

Starting from a partial differential equations (PDEs) setting, a delay differential equations (DDE) model is derived for an easier and more realistic approach and this is the man advantage of this model.

Finally, their equations also include interactions of tumor cells with immune system effectors.

In 2013, Heiko Enderling Integrated Mathematical Oncology H. Lee Moffitt Cancer Center and Research Institute .

They use ordinary differential equation, partial differential equation, tumor modeling, angiogenesis.

In ODE:

The number of cancer cells in a tumor is difficult to estimate due to constant changes in time. They can assume that the probability of this cell to divide within the time frame of one hour is 1/24. Not knowing the exact number of cells in a tumor population. (the disadvantage of this model). The number 24 is an assumption to the cell cycle length of an arbitrary cancer cell. But, The most apparent shortcoming of this approach is the lack of spatial consideration.

In PDE:

The model simulates cancer invasion and metastatic spread (which are two crucial and inherently spatial processes) by using partial differential equations. The equation for n therefore involves the partial derivatives of its independent variables. Omitting the considered spatial domain. they also can simulate the results and see the gap between the advancing tumor front and the receding tissue.

This can be considered as an improvement over the previous model.

In 2017, An extended dynamic model with time delay is developed to describe interactions between cancerous tumor and the adaptive immune system in mouse

The proposed model here explains dynamics of different agents from the first day of immune response to the cancer cell growth with the cell division program of immune cells considered, A protocol for immunotherapy with DC vaccine is also optimized.

In 2018, A hybrid three-scale model of tumor growth

This model enables investigation of different mechanisms rules at multiple scales on tumor progression. The strategy allows representing both the collective behavior due to cell assembly as well as microscopic intracellular phenomena described by signal transduction pathways.

The model goal was to capture the hallmarks of cancer including the ability of tumor cells to stimulate their own growth, replicate indefinitely, resist apoptosis, evade growth suppressors, and invade local tissue.

In 2019, Iranian Journal of Science and Technology, Transactions A: Science (2019) 43:687–700 [6]

(Various Mathematical Models of Tumor Growth with Reference to Cancer Stem Cells)

Very little has been done in the field of cancer stem cells. Herein, they have reviewed some mathematical models of tumor growth and their specific properties. Considering the importance of the role cancer stem cells play in the production, progression and recurrence of cancer, they have also examined a mathematical growth model describing the dynamics of tumor growth in the presence of cancer stem cells. Which is an integral part that differentiates it from past researches.

In 2021, Applied Science and Computer Mathematics 2(2), (2021), 11-20 w

(Some Applications of Partial differential Equations on Cancer Research)

In this research they introduce some other tumor growth models which deal with Partial Differential Equations (PDEs). Usually, the models of tumor growth consisting of a coupled system of PDEs whose spatial domain is the tumor that changes in size over time and gives some ideas on relation between such equations and tumor growth of cancer cells. In this paper, which is a collection of some PDEs extracted from several papers, they show how PDEs help to provide mathematical models in tumor growth, all while improving on the implementation of previous models.

Mathematical Modeling

Here we present mathematical models that are most often used to describe the proliferation of tumor inside the human body and to better understand how it grows, and to eventually reach to a better response to treatment and to make it even earlier.

Development of those models is based on some biological assumption.

ODE Modeling:

Tumor growth is a very complex system that can be simplified using ordinary differential equations.

There are many models but one the most common are the logistic Model and the Gompetz Model, those models were introduced to explain the behavior of cancer cell growth and proliferation with time to help researchers and doctors understand patient prognosis and the effectiveness of certain therapies.

Those models don't not deal with individual cells, but the population of the tumor as a whole.

Logistic Model→

$$\frac{\partial V_L}{\partial t} = r_L\left(1 - \frac{V_L}{K_L}\right)V_L, \qquad V_L(0) = V_{L0}$$

Gompertz Model→

$$\frac{\partial V_G}{\partial t} = r_G \ln\left(\frac{K_G}{V_G}\right)V_G, \qquad V_G(0) = V_{G0}$$

Where:

$V_L(t)$ & $V_G(t)$ are the tumor volumes (μm^3) as a function of time (day).

r_L & r_G are tumor growth rate constants (day^{-1}).

K_L & K_G are the carrying capacity (maximum capacity tumor can reach) (μm^3).

V_{L0} & V_{G0} are the volumes of the tumor at the time of initial observation (μm^3).

Both Models show that:

- Tumor growth decreases with time.
- Tumor growth is proportional linearly with size until the growth of the cells reaches the carrying capacity.
- When the tumor volume V(t) = K, $\frac{\partial V}{\partial t}$ will equal zero, which means that the tumor growth will stop when the tumor volume reaches its' maximum size.

- The growth rate is limited by the carrying capacities due to competition between cells for space and nutrients.

PDE Modeling:

ODE models can be considered as a fairly accurate representation of tumour growth with time, but it lacks spatial consideration, as in patients usually don't die of the cancer cells itself, but die because the cells invade and spread(metastasis) to different parts of the body and cause the growth of other tumours. Cancer invasion and spread are spatial processes, that can be represented by PDEs.

Firstly, we will discuss the first spatial model of cancer invasion, which is said to be developed by (i) Gatenby and Gawlinski. It explores the relation between H+ ions, normal tissue and cancer cells. Secondly, we will be looking at (ii) Wodarz's model et al. which represents the competing effects of an angiogenesis promoter and an inhibitor, and their effect on cancer cells growth. After that we will be looking at the model made by (iii) Ferreira et al., where he delves deeper into the effects of nutrient distribution on the mitosis and cell survival of cancer cells. For the 4th PDE we will look at the breast cancer's growth and invasion rate using models adapted from Anderson's model. Finally, we review a system of PDEs describing the spread and growth of the most malignant brain tumour: glioblastoma, also known as (GBM).

Gatenby and Gawlinski model is where the number of cancer cells is represented by n as a fraction (0-1) or percentage (0-100%) of the maximum available volume at this position at spatial positions either 1D(x), 2D(x,y), or 3D(x,y,z) space. Therefore, n is dependent on time and spatial dimensions. Considering the effects of H+ ions in the degradation of local tissue, so cancer cells can occupy the now empty space proliferate. (i) The following system of partial differential equations is used to model the spatiotemporal evolution of cancer cells, c, H+ ions, m, and extracellular matrix (or normal host tissue), v:

- $\partial c/\partial t = nonlinear\ diffusion + logistic\ growth$

$= \nabla[Dc\,(1-v)\nabla c] + \rho c(1-c),$ (1)

- $\partial m/\partial t = diffusion + production \& decay$

  $= \nabla\, 2m + (c-m),$ (2)

- $\partial v/\partial t = logistic\ growth\ degradation$

  $= (1-v) - \gamma mv,$ (3)

Dc is the diffusion coefficient, ρ is the cancer proliferation rate, δ represents the H+ ions production rate/decay rate & γ is the extracellular matrix degradation rate. From the previous equations, cancer cells proliferate, experience nonlinear diffusion and secrete H+ ions, but the diffusion rate depends on the density of the normal tissue surrounding it. Higher density of normal tissue = lower rate of diffusion and vice versa. The H+ ions diffuse and degrade the surrounding normal tissue. The H+ ions linearly decay while the normal tissue grows logarithmically in order to replace the degraded normal tissue.

Finally, we will introduce PDE Model for brain tumor :

Using a combination of computational simulation and the travelling wave theory of the aforementioned system of PDEs, Gatenby and Gawlinski anticipated the existence of a hypocellular gap at the interface between the normal and cancerous tissue. Later models delved deeper into this idea, to test the relation between cancer cells, c, degrading enzymes, m, and tissue, v, using reaction-diffusion-taxis models. Which is where the process of hap to taxis played a key role in the cancer cell migration. Hap to taxis is the directed cell migration in response to gradients of extracellular matrix density or gradients of adhesive molecules in the extracellular matrix.

The following model developed by Wodarz et al presents a multifocal tumour growth dependent on the competing effects of an inhibitor and an angiogenesis promoter. Where the cancer cells population ‘C’ produces promoter ‘P’ and inhibitor ‘I’. And the growth rate of the cancer cell population depends on the local blood supply which is considered as an increasing function of ‘P’ and a decreasing

function of 'I'. We consider that the spread of promoter is negligible, the cancer cells migrate and that the inhibitor diffuses:

$$\frac{\partial C}{\partial t} = \left(\frac{rC}{\epsilon c + 1}\right)\left(\frac{P}{I + 1}\right) - \mathcal{S}C + D_c \frac{\partial^2 C}{\partial x^2}$$

$$\frac{\partial p}{\partial t} = a_P c - b_p P$$

$$\frac{\partial I}{\partial t} = a_I C - b_I I - D_I \frac{\partial^2 I}{\partial x^2}$$

Where the production rates of promoter=aP and inhibitor=aI respectively by the tumour cells and bP, bI is their decay rates. The intrinsic growth rate of the cancer cells is represented by r and the parameter describing growth saturation with increasing tumour size is ε. The death rate of the cancer cells is δ and their migration rate is represented by DC. And finally, the diffusion rate of the inhibitor is shown as DI. We assume that such that the promoter is in quasi-equilibrium with the cancer cell population, which means that the dynamics of the production and decay of the promoter are fairly rapid (i.e. P = aPC/bP). Substituting this into the system of PDEs gives us a system of two coupled PDEs for C and I. Where we assume that they satisfy the zero flux boundary conditions. Furthermore, the equations have a stable.

Periodic and consist of peaks of cancer cell number. Where a1 is the bifurcation parameter, and if it is large, then the system falls to the zero-steady state. As a1 decreases the cancer cells have the ability to grow, but are limited to a single peak in the middle of the domain, due to the secretion of inhibitors that stop the cancer cells from growing elsewhere. The further decrease of a1's value only prevents cancer cell growth in the more immediate periphery of a peak of cancer cells and multiple tumor foci can form within the domain. As the strength of inhibitor decreases the distance between lesions decreases. Once a1 becomes sufficiently small, tumor cells have the ability to invade the whole space causing the spatially homogeneous positive steady state to be considered stable.

(iii) Tumor growth and the dynamics of the immune system have been a significant focus for mathematical modelling over the past three decades. Evolving from the early chemical diffusion and differential equation models of Burton and Greenspan, descriptions of tumor growth have been presented more recently using PDEs. There is A number of mathematical models have coupled tumor growth with immune system dynamics. Usually, these models are fully deterministic, comprised of a series of ODEs or PDEs describing the dynamics of (tumor cells, host cells, and immune cells).in this model we introduce the nutrient limited growth of an early-stage tumor and the dynamic interplay between the immune system and the growing tumor. The model involves a combination of reaction-diffusion equations for the nutrient species and numerous rules of evolution for the cellular automaton description of the various cell-types that comprise the tissue-tumor environment, that used in this model to describe the distribution of two chemicals necessary for mitosis and cell survival. As in the work of Ferreira et al, two nutrient species been considered. The first nutrient being a necessary component of the cell division processes, while the second is essential for cellular survival. The nutrients diffuse throughout the tissue space, and as they do so they are consumed by the different cells that are resident in tissue.

The nutrient species are governed by the following equations:

$$\partial N/\partial t = D_N \cdot [\nabla\_N]^2 N - k_1 HN - k_2 TN - k_3 IN. \quad (7)$$

$$\partial M/\partial t = D_M [\nabla\_M]^2 M - k_1 HM - k_2 TM - k_3 IM \quad (8)$$

where N and M represent the proliferation nutrient and survival nutrient, respectively.

and their diffusion coefficients are DN and DM. T for tumor cells, and I for immune cells.

K_1, K_2 and K_3 are the rates of consumption of proliferation nutrient by host cells, tumor cells and immune cells, respectively, while K_4, K_5, and K_6 are the corresponding rates for the survival nutrient.

(iv) The pattern of growth of human breast cancers is clinically important, specifically for estimating the duration of pre-diagnosis silent growth and for the design of an optimal post-surgery chemotherapeutic schedule

Mathematical models for the growth and invasion of breast cancer tumors into the surrounding tissue, together with modelling frameworks for surgery and radiotherapy were first developed by Anderson et al. [7]. To simulate breast cancer growth prior to diagnosis and quantify the effects of conventional fractionated radiotherapy versus more targeted irradiation, Anderson et al. initially developed a continuum model of ODEs and PDEs [9].

A basic description of the model incorporating the effects of radiotherapy is given as following form:

$$\partial n/\partial t = \lambda n(1-n-f) + dn \nabla^2 n - \gamma \nabla.(n \nabla f) \quad (9)$$

$$\partial f/\partial t = -\eta m f \quad (10)$$

$$\partial m/\partial t = dm \nabla^2 m + \alpha n(1-m) - \beta m \quad (11)$$

The system of equations describing the interactions of tumor cells (n), extracellular matrix (f), and matrix-degrading enzymes (m) is illustrated in the first equation. Therein, the terms in the first equation correspond to cellular proliferation, random motility and hap to taxis, defined in the model as the movement of tumor cells according to gradients of chemicals in the tumor environment. The second equation corresponds to the extracellular matrix degradation by existing tumor cells. Lastly, the terms in the third equation correspond to the diffusion of matrix degrading enzymes secreted by the tumor cells, the production of new enzymes and natural decay. It is not easy to find an analytical solution of the system of equations, if exists. However, an approximate solution can be constructed using an appropriate discretization scheme.

Solution And Analysis:

Here we focus mainly on the Warburg effect, and its mathematical modelling by using the typical strategy of acidity increasing against the environment operated by tumours to regulate their growth. Since no analytical results for the Gatenby-Gawlinski model is available or supportive, we will also explore its multidimensional framework in order to fill that gap. But before we start describing a mathematical model for tumor growth, we need to explain a biomedical phenomenon known as the Warburg effect. Otto Warburg confirmed using many experiments, that the tumor cells metabolise anaerobically even in the presence of huge amounts of oxygen. This process produces less energy than the traditional oxidative phosphorylation pathways taken my normal cells. Moreover, the glycolysis by tumor cells induces lactic acid fermentation. The key point of the analysis made in this article is the above-mentioned acid-mediated invasion hypothesis.

One critical assumption that we implement in this article is that the acidification caused by the lactic acid produced by the cancerous cells is advantageous for the cancer cells, while being toxic to the normal cells. The original model that is based on the reaction-diffusion equations made by Gatenby and Gawlinski is suitable for performing numerical investigations of the above phenomena.

The Gatenby-Gawlinski model:

Gatenby and Gawlinski is developed in order to reproduce cancer cells invasion within a healthy tissue, starting from a stage in which the carcinogenesis has already happened and, then, it is not further taken into account. Although interaction between malignant and health cell populations occurring at the tumor-host interface, and lactic acid an important role because of the glycolytic metabolism

$$\frac{\partial U}{\partial t} = \rho 1\, U\left(1 - \frac{U}{K}\right) - \delta 1\, UW$$

$$\frac{\partial V}{\partial t} = \rho 2\, V\left(1 - \frac{V}{K2}\right) + D2\, \frac{\partial}{\partial t}\left[\left(1 - \frac{U}{K1}\right)\frac{\partial V}{\partial x}\right.$$

$$\frac{\partial W}{\partial t} = \rho 3\, V + D3\, \frac{\partial^2 W}{\partial x^2} - \delta 3\, W$$

Which U and V are a logistic growth, with carrying capacity k_1,k_2 respectively. ρ_1, ρ_2 are growth rates δ_1 is a death rate proportional to W this term being involved to reproduce healthy cells degradation due to the interactions with the lactic acid.
The second equation describe the degenerate diffusion that is important for tumor cells density the coefficient D_2 stands for a diffusion constant of the neoplastic tissue when there is a complete lack of healthy tissue.

Note: No tumor spreading is allowed unless the surrounding healthy cells concentration is no longer equal to its carrying capacity that aim to simulate a realistic defence mechanism regarding tumor confinement, in addition to proliferation of both U and V as regulated by their combination or rather competition.

D3 is the spatial spreading of the lactic acid, ρ_3 is involved for the acid production that is linearly proportional to V, δ_3 is a physiological reabsorption rate.
In order to deal with more manageable quantities, it is advisable making the system non-dimensionalized, so that we have :

$$\frac{\partial u}{\partial t} = \mathbf{u}(\mathbf{1} - \boldsymbol{u}) - \boldsymbol{d}\,\boldsymbol{uw}$$

$$\frac{\partial V}{\partial t} = \mathbf{rv}\,(\mathbf{1} - \boldsymbol{v}) + \boldsymbol{D}\,\nabla.[(\mathbf{1} - \boldsymbol{u})\,\nabla \boldsymbol{v}]$$

$$\frac{\partial W}{\partial t} = \mathbf{c}(\mathbf{v} - \mathbf{w}) + \nabla^{\mathbf{2}}\boldsymbol{w}$$

This resultant version allows to operate with fewer (positive) parameters d, r, D and c, thus reducing their original range and coping with scaled functions u(x, t), v(x, t) and w(x, t) at $t \geq 0$.

To identify the key qualitative features of wave propagation, a comprehensive study of the traveling fronts associated to the Gatenby-Gawlinski model is performed conditions for the appearance of a tumor host interstitial gap are provided, thus confirming and extending the estimates proposed in (Gatenby, R.A., Gawlinski, E.T.: A reaction-diffusion model of cancer invasion) and in (Gatenby, R.A., Gawlinski, E.T.: The glycolytic phenotype in carcinogenesis and tumor invasion: insights through mathematical models).

Numerical Solution and algorithm:

We will solve the equations using numerical strategy that based on cell centered finite volume approximations for the spatial discretization.

The finite volume method is suitable to be the way to solve the equations as the integral formulation of the system equations, is a suitable ground to guarantee consistency in terms of closeness to the physics of the model. We will firstly derive semi -discrete finite volume approximation, and use the general case using non-uniform mesh. We will assume that

$$Zi = [Xi - \frac{1}{2}\ , Xi + \frac{1}{2}]$$

Is the finite volume centered at Xi, where

$$Xi = \frac{Xi - \frac{1}{2} + Xi + \frac{1}{2}}{2}$$

for I = 1, 2, ..…. N. where N is a fixed number of vertices to be selected on the one-dimensional mesh.

We will make ΔX to be the (variable) spatial mesh size;

Where

$$\Delta Xi = |Xi + \frac{1}{2} - Xi - \frac{1}{2}|$$

So that

$$|Xi - Xi - 1| = \frac{\Delta Xi - 1}{2} + \frac{\Delta Xi}{2}$$

and this Will be the typical length for an interfacial interval

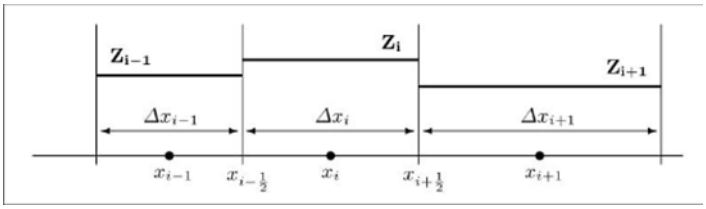

We will solve firstly the equation of the healthy tissue density and examine it is finite volume integral version

$$\frac{1}{\Delta Xi}\int_{zi}\frac{\delta u}{\delta t}(x,t)dx = \frac{1}{\Delta Xi}\int_{zi} u(x,t)\big(1-u(x,t)\big)dx - \frac{d}{\Delta Xi}\int_{zi} u(x,t)w(x,t)dx$$

finite volume integral averages

$$ui(t) = \frac{1}{\Delta Xi}\int_{zi} u(x,t)dt$$

And semi discrete equation become

$$\frac{d}{dt}ui(t) = u(t)(1 - ui(t)) - dui(t)w(t)$$

Similarly, the equation for the tumor cells density in will be

$$\frac{1}{\Delta Xi}\int_{zi}\frac{\partial u}{\partial t}(x,t)dx$$
$$= \frac{r}{\Delta Xi}\int_{zi} v(x,t)\big(1-v(x,t)\big)dx$$
$$+ \frac{D}{Xi}\int_{zi}\frac{\partial}{\partial x}\left[\big(1-u(x,t)\big)\frac{\partial u}{\partial x}(x,t)\right]dx$$

We will rearrange the equation for the finite volume integral of the diffusion term.

And proceed this by evaluating the differential term at the mesh interfaces as follow:

$$\frac{D}{\Delta Xi}\left[\left(1-u\left(xi+\frac{1}{2}\right)\right)\frac{\partial u}{\partial x}\left(xi+\frac{1}{2},t\right)-\left(1-u\left(xi-\frac{1}{2},t\right)\right)\frac{\partial u}{\partial x}\left(xi-\frac{1}{2},t\right)\right]$$

$$\approx \frac{D}{\Delta xi}\left[\frac{\big(1-ui(t)\big)\Delta xi+\big(1-u_{i+1}(t)\big)\Delta x_{i+1}}{\Delta xi+\Delta x_{i+1}}\cdot\frac{v_{i+1}(t)-vi(t)}{\frac{\Delta xi}{2}+\frac{\Delta x_{i+1}}{2}}\right.$$

$$\left.-\frac{\big(1-u_{i-1}(t)\big)\Delta x_{i-1}+(1-ui(t)))\Delta xi}{\Delta x_{i-1}+\Delta xi}\cdot\frac{vi(t)-v_{i-1}(t)}{\frac{\Delta x_{i-1}}{2}+\frac{\Delta xi}{2}}\right]$$

After that we will approximate the interfacial quantities by building weighted averages, whose weights are the size of the adjacent finite volumes,

so that Δxi/Δxi+1 and Δxi−1/Δxi are employed at the interfaces xi+1/ 2 and xi−1/ 2, respectively.

And the upwind formula (which makes use of the function evaluations at the neighboring vertices) makes the first order derivative of v(t) are discretized.

Finally, the equation of lactic acid

$$\frac{1}{\Delta xi}\int_{zi}\frac{\partial w}{\partial t}(x,t)dx$$

$$=\frac{c}{\Delta xi}\int_{zi}v(x,t)dx-\frac{c}{\Delta xi}\int_{zi}w(x,t)dx+\frac{1}{\Delta xi}\int_{zi}\frac{\partial^2 w}{\partial x^2}(x,t)dx$$

by proceeding as for the previous cases, the approximation equation will be as follow

$$\frac{d}{dt}wi(t)=c\big(vi(t)-wi(t)\big)+\frac{1}{\Delta xi}\left[\frac{w_{i+1}(t)-wi(t)}{\frac{\Delta xi}{2}+\frac{\Delta x_{i+1}}{2}}-\frac{wi(t)-w_{i-1}(t)}{\frac{\Delta x_{i-1}}{2}+\frac{\Delta xi}{2}}\right]$$

And this equation in case of uniform mesh can be

$$\frac{d}{dt}wi(t) = c\big(vi(t) - wi(t)\big) + \frac{wi + l(t) - 2wi(t) + wi - l(t)}{\Delta X^2}$$

And for simplicity we will make the quantity delta X to be constant, so $\Delta xi = \Delta x$ for all i= 1, 2,.... N.

Then the semi –discrete version of the cancer equation becomes

$$\frac{d}{dt}vi(t) = rvi(t)\big(1 - vi(t)\big) + \frac{D}{\Delta x}\Big[\frac{\big(1 - ui(t)\big) + \big(1 - u_{i+1}(t)\big)}{2}.\frac{v_{i+1}(t) - vi(t)}{\Delta x} - \frac{\big(1 - u_{i-1}(t)\big) + \big(1 - ui(t)\big)}{2}.\frac{vi(t) - v_{i-1}(t)}{\Delta x}\Big]$$

And after some approximation and some conventional manipulation it can be as follows:

$$\frac{d}{dt}vi(t) = rvi(t)\big(1 - vi(t)\big) + \frac{D}{\Delta x^2}\big[\big(1 - ui(t)\big)\big(v_{i+1}(t) - 2vi(t) + v_{i-1}(t)\big) - \frac{1}{2}\big(v_{i+1}(t) - vi(t)\big)\big(u_{i+1}(t) - ui(t)\big) - \frac{1}{2}\big(vi(t) - v_{i-1}(t)\big)\big(ui(t) - u_{i-1}(t)\big)\big]$$

For general solution

- $\boldsymbol{u_i^{n+1} = u_i^n + \Delta t\,[u_i^n(1 - u_i^n) - du_i^n w_i^n]}$

- $\boldsymbol{u_i^{n+1} = u_i^n + r\Delta t\, u_i^n(1 - u_i^n) + D\frac{\Delta t}{\Delta x^2}\Big[\big(1 - u_i^{n+1}\big)\big(v_{i+1}^{n+1} - 2\,v_i^{n+1} + v_{i-1}^{n+1}\big) - \frac{1}{2}\big(v_{i+1}^{n+1} - v_i^{n+1}\big)\big(u_{i+1}^{n+1} - u_i^{n+1}\big) - \frac{1}{2}\big(u_i^{n+1} - u_{i-1}^{n+1}\big) - \frac{1}{2}\big(u_i^{n+1} - u_{i-1}^{n+1}\big)\Big]}$

- $\boldsymbol{w_i^{n+1} = w_i^n + c\Delta t(v_i^n - w_i^n) + \frac{\Delta t}{\Delta x^2}\big(w_{i-1}^{n+1} - 2w_i^{n+1} + w_{i+1}^{n+1}\big)}$

For n = 1, 2,...., Neumann-type boundary conditions are also applied. In compared to purely explicit algorithms, which are heavily constrained by the constraints that stability usually requires, this explicit-implicit mixed approach forces us to make less pricey time step choices. The possibility of using fully implicit schemes was considered, but it was ultimately rejected because no significant accuracy in approximation would have been gained, only an increase in computational time. We highlight that, in order to efficiently solve the discrete system, it is useful to begin with the solution u^{n+1} for the healthy tissue, whose treatment turns out to be fully explicit; then, by utilising the block-matrix structure arising from the other equations, a reciprocal independence between the solutions$v^{n+1} and\ w^{n+1}$ and is produced.it is easy to go ahead solving separately the corresponding equations and getting the global approximation evaluated at the discrete t^{n+1}

Space-averaged propagation speed approximation

After a numerical solution as shown to proceed with experiments and simulations consists in defining a useful tool for the wave speed estimation of the numerical solutions. With the aim of providing a numerical approximation for the wave speed at time t^n, we employ a space-averaged estimate which applied to the case of a reactive version of the Goldstein- Kac model for correlated random walk.
To provide the main analytical concepts behind the numerical formulation of the wave speed estimation, we briefly derive its analytical counterpart by means of some standard manipulations. Let ϕ b a differentiable function describing the traveling front profile

$$\int_R [\emptyset(\varepsilon + h) - \emptyset(\varepsilon)]d\varepsilon = h \int_R \int_0^1 \frac{\partial \emptyset}{\partial \varepsilon}(\varepsilon + \theta h)d\theta d\varepsilon = h \int_0^1 \int_R \frac{\partial \emptyset}{\partial \eta}(\eta)d\,\eta d\theta$$

$$= h \int_0^1 [\emptyset(+\infty) - \emptyset(-\infty)]d\theta = h(\emptyset_+ - \emptyset_-),$$

where h > 0 is an increment, At this stage, setting h = -sΔt, we deduce the following integral equation for the wave speed

$$s = \frac{1}{[\emptyset]\Delta t} \int_R [\emptyset(\varepsilon) - \emptyset(\varepsilon - s\Delta t)]d\varepsilon,$$

by imposing the synthetic notation $[\phi] := \phi_+ - \phi_-$
the space-averaged wave speed estimation for v(x; t) over a uniform spatial mesh at time t^n is given by $s^n = \frac{\Delta x}{[\emptyset]\Delta t}\sum_{i=1}^{N}\left(v_i^n - v_i^{n+1}\right)$,

With ϕ + and ϕ- that are prescribed as stationary states of the equation for v(x; t) inside the dynamical system underlying

Multidimensional Simulations

One-dimensional simulation results

We will use this scheme for numerical simulation:

- $\boldsymbol{u_i^{n+1} = u_i^n + \Delta t\,[u_i^n\,(1 - u_i^n) - d u_i^n u w_i^n]}$
- $\mathbf{v_i^{n+1} = v_i^n + r\Delta t\, v_i^n\,(1 - v_i^n) + D\frac{\Delta t}{\Delta x^2}\Big[(1 - u_i^n)\left(v_{i+1}^{n+1} - 2v_i^{n+1} + v_{i-1}^{n+1}\right) - \frac{1}{2}\left(v_{i+1}^{n+1} - v_i^{n+1}\right)\left(u_{i+1}^{n+1} - u_i^{n+1}\right) - \frac{1}{2}\left(v_i^{n+1} - v_{i-1}^{n+1}\right)\left(u_i^{n+1} - u_{i-1}^{n+1}\right)\Big]}$
- $\boldsymbol{w_i^{n+1} = w_i^n + c\Delta t(v_i^n - w_i^n) + \frac{\Delta t}{\Delta x^2}\left(w_{i-1}^{n+1} - 2w_i^{n+1} + w_{i+1}^{n+1}\right)}$

with Neumann-type boundary $u_1^n = u_2^n, v_1^n = v_2^n \; and \; w_1^n = w_2^n$, for n = 1, 2, 3,4,.... ,n are also implemented.

together with formula: $s^n = \frac{\Delta x}{[\emptyset]\Delta t}\sum_{i=1}^{N}(v_i^n + v_i^{n+1})$, for the wave speed estimation. Therefore the experiments are carried out with the scaled parameters as listed in Table 1.

Table 1. Numerical values for the simulation parameters:

d	r	D	c	L	T
{0.5, 1.5, 2.5, 3, 12.5}	1	$4 * 10^{-5}$	70	1	20

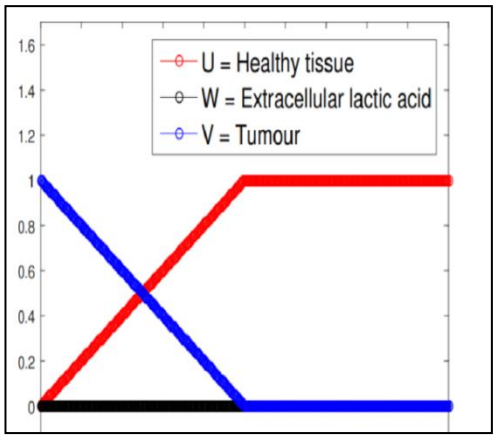

we assume T as the final time instant, while the spatio-temporal mesh is built by fixing $\Delta x = 0.005$ and $\Delta t = 0.01$. For the choice of the initial profiles, a piecewise linear decreasing density is taken into account for the cancer cells extending out from its core, where v = 1, and getting towards zero; for the healthy cells density, the starting graph is simply obtained through a reflection, by imposing a complementary behaviour with respect to the cancer cells density; finally, the extracellular lactic acid. Concentration is initially equal to zero. The corresponding graphs are shown in **Figure1**. We will notice from the simulation that there are two different types of behaviours which are regulated by the parameter d measuring the destructive influence of the environment acidity on the healthy tissue, and so taken as an indicator of the tumor aggressiveness.

A. When d<1(Figure 2.a): It is characterized by the coexistence of tumor and healthy tissue behind the wave front, because a fraction of normal cells survives to the chemical action of the tumor thanks to low sensitivity to the environment acidity. Acid concentration immediately attains its carrying capacity at the left-hand boundary, and finally the level of the healthy cells density is exactly 1 − d in the purely heterogeneous case.

B. When d>>1 (Figure 2.d): That is the most aggressive configuration. Indeed, the healthy tissue is being completely destroyed behind the advancing tumor cells wave front because of the high level of acidity induced into the environment.

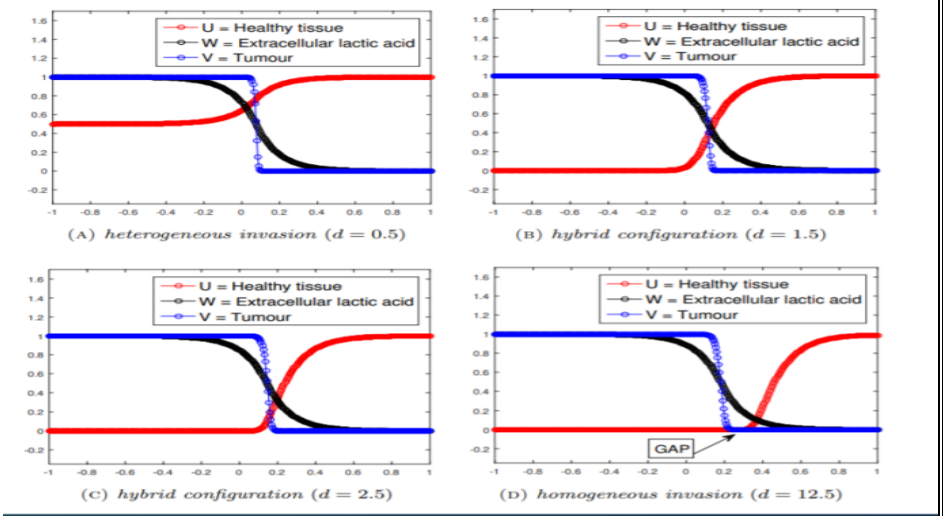

A narrow overlapping zone actually persists for increasing values of d > 1, which produces hybrid configurations

as shown in Figure 2(B) and Figure 2(C), but it reduces progressively .Remarkable feature of the last configuration is the presence of a tumor-host hypo cellular interstitial gap , namely a separation zone between the healthy and cancer cells populations.

From a mathematical point of view, the strong dissimilarity in terms of steepness of the wave profiles for the healthy and tumors densities observed in Figure 2 is justified by the fact that somehow U inherits the (parabolic) regularity of the acid concentration W through the reaction term, whereas the diffusion constant D of the neoplastic tissue is typically very small (refer to Table 1).

As a matter of fact, the parameter is deduced as D = D2/D3 and it is physically relevant to assume that D3 is much larger than D2. Therefore, the tumor propagating front V is normally steeper, despite its diffusivity (hindered by U through a degenerate factor) is selected as the driving mechanism of invasion, since no diffusion is considered for the healthy cells due to their epithelial phenotype. Indeed, the wave front U fails to keep its regularity once the equation for W is removed.

Another effect on the shape of the wave profiles can be appreciated dealing with the dimensional parameter r, which is expected to be greater than 1 since deduced as r = ρ2/ρ1 from physical considerations (we report in Figure 3 the numerical simulation of an experimental case) .

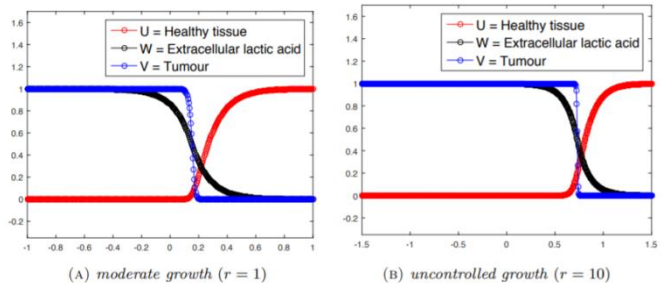

(A) *moderate growth* ($r = 1$) (B) *uncontrolled growth* ($r = 10$)

Figure 3

We have attempted a qualitative comparison with the analytical results by computing numerical solutions using the parameters listed in **Table 2**. In particular, we are interested in tracking the formation of the interstitial gap, whose appearance is expected for d > 2 (in which case its size can also be estimated).

The numerical simulations reported in Figure 3 actually corroborate such prediction, although some discrepancies emerge concerning the smoothness of the wave profile for the healthy cells density, thus determining a smaller size for the gap separating the host and tumor populations. Besides the effects of a bigger diffusion constant D for the tumor cells, which slightly smooth out the steepness of the propagating fronts, we must recall that the analysis is based on asymptotic expansions and, therefore, solely the leading terms contribute to shape the solution profiles (this comment applies also to Figure 3).

Table 2. Numerical values for the simulation parameters:

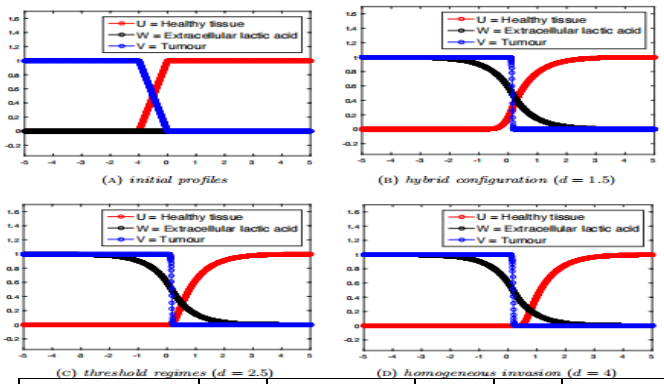

(A) *initial profiles* (B) *hybrid configuration* ($d = 1.5$)

(C) *threshold regimes* ($d = 2.5$) (D) *homogeneous invasion* ($d = 4$)

d	r	D	c	L	T
{1.5, 2.5, 4}	1	$4 * 10^{-5}$	2	5	20

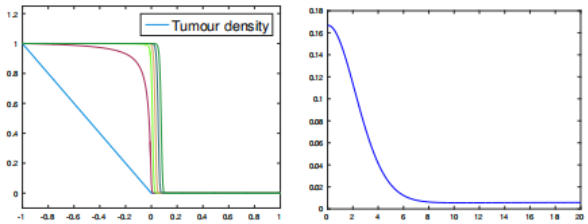

(A) *front evolution* (B) *wave speed estimates*

Figure 4

1-As mentioned above, the existence of the propagating fronts is a key point and It is essential for our investigation and information about its wave speed.

2-to quantify these values, we take advantage of the space-averaged propagation speed approximation:

$\mathbf{S_n} = \frac{\Delta x}{[\emptyset]\Delta t} \sum_{i=1}^{N} (Vi^{n} - Vi^{n+1})$, with $\emptyset$ is prescribed as stationary states of the equation for v(x, t) **(eq2).** and we apply it to better understand the wave front behavior of the Gatenby-Gawlinski model

investigation case	Numerics	Analytical wave speed	Relative Error
Homogeneous	0.0124	$s \approx 2\sqrt{Dr}=0.0126$	0.0159
Heterogeneous	0.0058	$s \approx 2\sqrt{Dr}=0.0063$	0.0794

Figure 5

1-the plot proposed in Figure 5 (A) is meant for capturing front evolution starting from the initial profile and, by means of Different colors, the tumor cells density function is plotted at different times until it reaches the shape of a propagating front defined by a stable wave speed. The graph in Figure 5 (B) shows the discrete wave speed estimate computed as a function of time, and it is possible to appreciate the convergence towards the asymptotic threshold; furthermore, it is easy to verify that a small waiting time is required before achieving an asymptotic value.

Table 3. Comparison between analytical wave speed formulations and the numerical estimates issued from (eq2)

1-In Table 3 the discrete asymptotic wave speed approximations issued from **(eq2)** are listed in order to make a comparison: in both the homogeneous and heterogeneous cases
2-We can deduce that numerical values are extremely near to the corresponding quantities computed using the analytical formulations. it is interesting to notice that, at least in the homogeneous case, the wave speed prediction $s \approx 2\sqrt{Dr}$ perfectly matches the analytical formula already known for the Fisher-KPP equation.

Two-dimensional experiments.

we delve deeper into the two different kinds of tumor invasion, which was previously described in section 5. Firstly, we consider the 2-ball of radius R centred at the point C, namely $\Omega = B_R(C)$, in the circular petri dish. We have taken R = 8 and C = (0,0) as simulation parameters. For the initial standing, we assume the evolution of a cancerous peak located in the origin of the petri dish, and the extracellular lactic acid concentration is initially assumed to be zero. For $x \in \Omega$, the corresponding functions are:

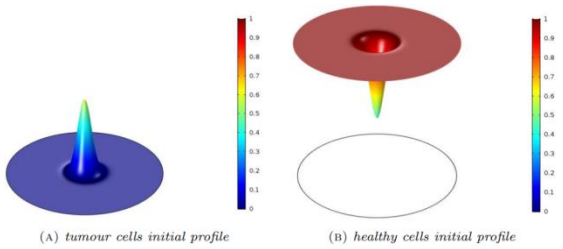

Plots of the initial profiles for tumor and healthy cells densities. Figure (6)

Numerical simulations have been performed until T = 13 and the time instant T = 6 has been selected for checking the progress of plots. The homogeneous invasion is the first case to be examined: In the next two figures tumor and healthy cells densities, respectively. Reported in First figure(A) and Second figure (A), the qualitative dynamics shows the initial cancerous peak growing and spreading out at the expense of the local healthy tissue.

The homogeneous invasion is the most aggressive situation, due to the complete annihilation of healthy cells behind the advancing radially headed cancerous core. It is possible that the local healthy tissue is not being completely repulsed by the tumor, in contrast to what observed in the second figure because healthy cells are destroyed through the strong effect of the lactic acid concentration. The next figure shows the healthy cells density reaches an asymptotic threshold within the inner region of the experimental domain, where the cancerous core is already detectable. The essential qualitative difference arising when comparing the two kinds of tumor invasion lies in the coexistence of healthy and cancer cells on one side (heterogeneous invasion), and the annihilation of the local healthy tissue out of the cancerous core on the other side (homogeneous invasion). In the homogeneous case, we have appreciated that there is not intersection between healthy and tumor cells densities. The healthy and tumor cells densities have been plotted simultaneously.

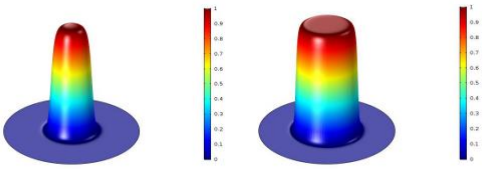

(A) *intermediate time* (B) *final time*

The homogeneous invasion: tumour cells density evolution at two different time instants $T=6$ (A) and $T=13$ (B).

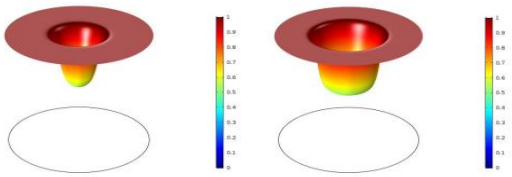

(A) *intermediate time* (B) *final time*

The heterogeneous invasion: healthy cells density evolution at two different time instants $T=6$ (A) and $T=13$ (B).

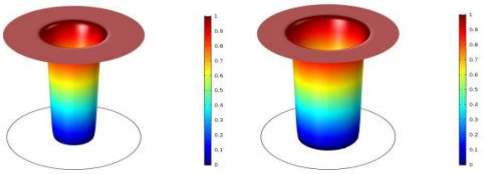

(A) *intermediate time* (B) *final time*

The homogeneous invasion: healthy cells density evolution at two different time instants $T=6$ (A) and $T=13$ (B).

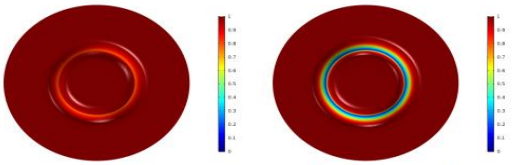

(A) *heterogeneous invasion* (B) *homogeneous invasion*

Identification of the two-dimensional *gap* formation for the homogeneous case (B) with respect to the heterogeneous case (A).

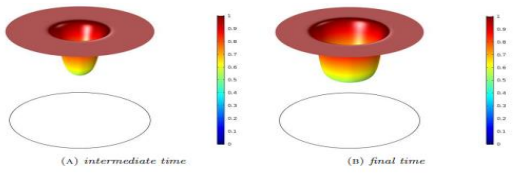

(A) *intermediate time* (B) *final time*

The heterogeneous invasion: healthy cells density evolution at two different time instants $T=6$ (A) and $T=13$ (B).

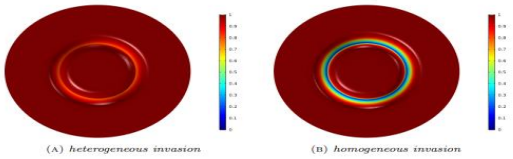

(A) *heterogeneous invasion* (B) *homogeneous invasion*

Identification of the two-dimensional *gap* formation for the homogeneous case (B) with respect to the heterogeneous case (A).

On the one hand, it is possible to appreciate the gap formation around the cancerous pick for the homogeneous invasion, as in the previous figure(B): a smaller blue ring, is recognizable within the circular crown located between the fronts. On the other hand, for the heterogeneous invasion, In figure (A) shows that healthy and tumor cells. Finally, we build a more complex configuration for the initial profiles made of three distinct cancerous peaks. The simultaneous plots of healthy and tumor cells densities at different time instants. We skip over the details concerning the single densities for analysing the gap evolution and for qualitatively interpreting the resultant dynamics of the fronts.

Three-dimensional experiments

Then we come to exploring the three-dimensional framework, we focus on the homogeneous invasion, in order to know the phenomenon of the spatial interstitial gap and the geometry of it. we use Para View for post- processing graphical results.

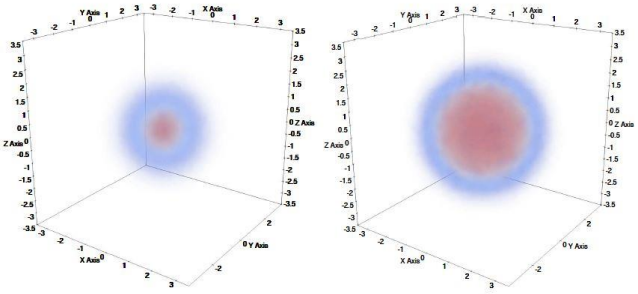

(A) *initial profile* (B) *intermediate time*

figure (10)

By analogy with the two-dimensional experiments, the 3-ball of radius R centered at the point C is chosen as the simulation domain, and we build the corresponding finite element mesh as shown in Figure 12(B) for the volume = BR(C) with R = 3:5 and C = (0; 0; 0), for instance. The three-dimensional version of the initial profiles given in (7.3) is also considered, and T = 7 is assumed as final time instant. All the plots are realized by exploiting a graphical heat map and setting the colour palette ranging from blue to red, as the magnitudes go from the lower values to the higher ones.

As concerns the qualitative evolution, the resulting dynamics displays the cancerous peak spreading out at the expense of the local healthy tissue, Figure 10(A) shows the cancer cells initial profile, while Figure 10(B) reports the evaluation at an intermediate time instant T = 4. By means of a transparency technique, that allows to appreciate the numerical data distribution throughout the three-dimensional volume, the tumor growth is suitably emphasized.

The final configuration for both healthy and cancer cells densities is depicted in Figure 11(A) and Figure 11(B), respectively, which shows Healthy and tumor cells densities evaluation at final time T =7

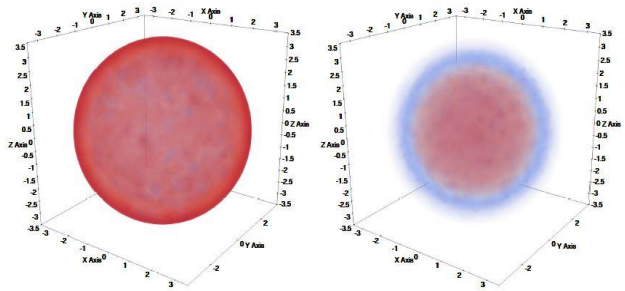

(A) *healthy cells density* (B) *tumour cells density*

figure (11)

Then we will have a look inside the volumes of Figure 11. For collecting information about the gap formation and understanding how the densities are distributed within the experimental domain. We cut the domain by means of a section plan passing through the origin and exploit the radial symmetry of the solutions to the system to state that any other section plan would produce similar results.

We report in Figure 12 the graphs corresponding to the half ball for both healthy and tumor cells densities, where the numerical data under examination are represented on the external spherical surface only.

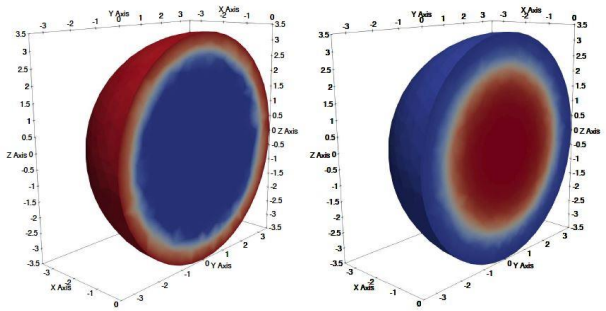

(A) *healthy cells density* (B) *tumour cells density*

figure (12)

This choice provides us with a clearer viewpoint to better detect the inner regions characterized by the distribution of different densities. Indeed, taking advantage of symmetry arguments, we can easily infer that data distributions arising from surface representation retain an analogous behaviour inside any inner layer. Moreover, the healthy cells density is identically null throughout a ball contained inside the domain (see Figure 12(A)), while the innermost cancerous core reveals itself in bright red (see Figure 12(B)).
As a matter of fact, Figure 12 turns out to be a sort of graphical proof for assessing the presence of a separation zone between the healthy and cancer cells densities, preventing them from being in touch as the evolution is going on. Therefore, available space emerges to include the tumor cell density without producing intersection, as it has been already observed for the one-dimensional and the two-dimensional framework.

Figure 13 shows a simultaneous plot consisting of numerical data merging from Figure11(B) and Figure 12(A), where the cancerous core is placed in its corresponding special domain with respect to the half ball provided with the healthy cells density profile throughout the external spherical surface.

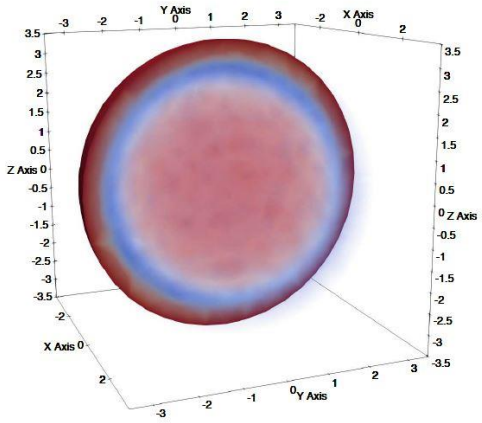

figure (13)

At this stage, identifying the three-dimensional version of the spatial interstitial gap becomes possible: we are dealing with a null density solid shell located between the healthy and tumor cells profiles, which is quite well recognizable in Figure 13**.**

Finally, in order to provide the most effective three-dimensional representation of the qualitative dynamics of the Gatenby-Gawlinski model, we have realized a meaningful simultaneous plot of Figure 11(A) and Figure 11(B) by exploiting the transparency technique, and the resulting graph is depicted in Figure 13, where the geometry of the spatial interstitial gap is now clearly noticeable.

[i] Reference

[1] National Cancer Institute. (2020, September 25). *Cancer statistics*. National Cancer Institute. Retrieved November 15, 2021, from https://www.cancer.gov/about-cancer/understanding/statistics.

[2] https://link.springer.com/content/pdf/10.1007/s002850050149.pdf

[3] https://www.sciencedirect.com/science/article/abs/pii/0025556494001173.

[4] G. Bocharov and K. P. Hadeler, Structured population models, conservation laws, and delay equations, Journal of Differential Equations, 168 (2000), 212–237.

[5] R. Nisbet and W. Gurney, The systematic formulation of population models for insects with dynamically varying instar duration, Theoretical Population Biology, 23 (1983), 114–135

[6] https://link.springer.com/content/pdf/10.1007/s40995-019-00681-w.pdf